Molecular Therapy
Nucleic Acids
Original Article

Scavenger Receptor Class A1 Mediates Uptake of Morpholino Antisense Oligonucleotide into Dystrophic Skeletal Muscle

Shouta Miyatake,[1] Yoshitaka Mizobe,[1] Maria K. Tsoumpra,[1] Kenji Rowel Q. Lim,[2] Yuko Hara,[1] Fazel Shabanpoor,[3,4] Toshifumi Yokota,[2] Shin'ichi Takeda,[1] and Yoshitsugu Aoki[1]

[1]Department of Molecular Therapy, National Institute of Neuroscience, National Center of Neurology and Psychiatry, Kodaira, Tokyo 187-8502, Japan; [2]Department of Medical Genetics, University of Alberta Faculty of Medicine and Dentistry, Edmonton, AB T6G 2H7, Canada; [3]The Florey Institute of Neuroscience and Mental Health, University of Melbourne, Parkville, VIC 3052, Australia; [4]School of Chemistry, University of Melbourne, Parkville, VIC 3010, Australia

Exon skipping using phosphorodiamidate morpholino oligomers (PMOs) is a promising treatment strategy for Duchenne muscular dystrophy (DMD). The most significant limitation of these clinically used compounds is their lack of delivery systems that target muscles; thus, cell-penetrating peptides are being developed to enhance uptake into muscles. Recently, we reported that uptake of peptide-conjugated PMOs into myofibers was mediated by scavenger receptor class A (SR-A), which binds negatively charged ligands. However, the mechanism by which the naked PMOs are taken up into fibers is poorly understood. In this study, we found that PMO uptake and exon-skipping efficiency were promoted in dystrophin-deficient myotubes via endocytosis through a caveolin-dependent pathway. Interestingly, SR-A1 was upregulated and localized in juxtaposition with caveolin-3 in these myotubes and promoted PMO-induced exon skipping. SR-A1 was also upregulated in the skeletal muscle of *mdx*52 mice and mediated PMO uptake. In addition, PMOs with neutral backbones had negative zeta potentials owing to their nucleobase compositions and interacted with SR-A1. In conclusion, PMOs with negative zeta potential were taken up into dystrophin-deficient skeletal muscle by upregulated SR-A1. Therefore, the development of a drug delivery system targeting SR-A1 could lead to highly efficient exon-skipping therapies for DMD.

INTRODUCTION

Duchenne muscular dystrophy (DMD) is a severe muscle disorder characterized by mutations in the *DMD* gene that primarily disrupt its reading frame, resulting in the absence of a functional dystrophin protein. A related allelic disorder, Becker muscular dystrophy, whose phenotype ranges from one very similar to that of DMD to almost asymptomatic, typically results from shortened but in-frame transcripts of *DMD* that allow for the expression of limited amounts of an internally truncated but partially functional protein.[1] One of the most promising therapeutic candidates for overcoming the absence of dystrophin in DMD is exon-skipping therapy using antisense oligonucleotides (ASOs), which modulate splicing patterns from out-of-frame to in-frame dystrophin transcripts. This therapy has been demonstrated to exclude specific exons, thereby correcting the translational reading frame, resulting in the production of "Becker-like," shortened, but partially functional proteins.[2] ASOs alter splicing patterns by targeting specific sequences in pre-mRNA elements involved in exon recognition and/or consensus splice sites.[3]

Phosphorodiamidate morpholino oligomers (PMOs), which are among the most promising ASOs, possess a morpholino rather than a ribose moiety and an uncharged phosphorodiamidate rather than a negatively charged phosphodiester linkage backbone. PMOs have been widely used to study gene function in non-mammalian animal models, such as zebrafish, frogs, and sea urchins.[4] Thus far, PMOs have demonstrated sufficient safety and efficacy in exon skipping for use in murine and canine models of DMD *in vivo*.[5–8] In addition, the U.S. Food and Drug Administration (FDA) recently approved Exondys 51 (eteplirsen) by Sarepta Therapeutics under the accelerated approval pathway as a PMO-based exon 51-skipping drug. This represents the first ASO-based treatment for DMD to be approved by the FDA.[9] However, its most significant limitation is the lack of a delivery system into myofibers. It has been reported that intravenously injected PMO remained detectable in the serum less than 2 h after injection (with a half-life of approximately 30 min), mainly owing to rapid renal clearance.[10–12] Therefore, it is essential to elucidate the molecular mechanism of cellular PMO uptake and establish a delivery system targeting skeletal and cardiac muscle fibers to obtain efficacy even with low doses.

However, the uptake mechanism for PMO with a neutral backbone, which possibly limits interactions with the cell surface necessary for endocytosis,[13] is unclear but is assumed to be ATP independent and the consequence of nonspecific passage through

Received 18 July 2018; accepted 19 January 2019;
https://doi.org/10.1016/j.omtn.2019.01.008.

Correspondence: Yoshitsugu Aoki, Department of Molecular Therapy, National Institute of Neuroscience, National Center of Neurology and Psychiatry, 4-1-1, Ogawa-higashi, Kodaira, Tokyo 187-8502, Japan.
E-mail: tsugu56@ncnp.go.jp

pores in damaged membranes based on the "leaky membrane" theory of muscles lacking dystrophin.[14,15] Intriguingly, we reported that PMO entry into myofibers is dependent on the developmental stage of myogenesis rather than on leaky membranes.[16] Consistently, Novak et al.[17] recently reported that systemically injected PMO localized to inflammatory foci, where it entered macrophages, actively differentiating between myoblasts and newly forming myotubes. Additionally, Han et al.[18] showed that co-administration of PMO with glucose enhanced exon-skipping activity in *mdx* mice, and that the uptake was mediated by energy-dependent endocytic pathways.

Furthermore, we recently demonstrated that scavenger receptor class A (SR-A) receptors mediate the uptake of a type of peptide-conjugated PMO, namely Pip6a-PMOs, into skeletal muscle.[19] SRs play a central role in innate immunity and homeostasis through the uptake of pathogen-associated and damage-associated molecular patterns.[20] They are subdivided into several classes, from A to I, which are structurally diverse but functionally similar in their ability to bind polyanionic particulate substrates, displaying clusters of cationic residues (cationic patches).[20,21] Their vast array of ligands includes oxidized low-density lipoprotein, acetylated low-density lipoprotein, apoptotic cells, *Staphylococcus aureus*, hepatitis C virus, lipopolysaccharide,[22] prion proteins, viral RNA, and different types of synthetic nanoparticles.[20,23,24] SRs are highly expressed in immune cells such as macrophages but are also expressed in other cell types, including skeletal and smooth muscle cells, endothelial cells, fibroblasts, splenic dendritic cells, and epithelial cells.[25,26] SR-As are among the most extensively studied SRs and are membrane glycoproteins with cationic collagenous domains at their ligand-binding sites.[27] SR-As have different subtypes, including SR-A1, SR-A2 (MARCO), SR-A3, SR-A4 (Colec12), and SR-A5. We found that all SR-As except SR-A2 were expressed in the murine C2C12 and H2K-*mdx* myoblast cell lines, and that their expression increased significantly throughout differentiation of both cell lines,[19] which correlated closely with the increased Pip6a-PMO uptake and activity accompanying their differentiation.[28]

Pip6a-PMO is a modified PMO-conjugated, cell-penetrating peptide containing multiple cationic arginines that enhance ASO delivery due to their unique ability to deliver cargo across plasma and endosomal membranes.[28,29] Importantly, we found that Pip6a-PMO has a high propensity to spontaneously self-assemble into nanoparticles in physiological buffers, and that the resulting micelles have a net negative charge (zeta potential), enabling their uptake into muscle cells by SR-As as anionic ligands.[19] However, whether naked PMO with a neutral backbone binds to SR-As is unknown.

In this study, we investigated the relationship between cell-surface SR-As and endocytic uptake of PMOs in dystrophic skeletal muscle, using the H2K-*mdx*52 myogenic cell line and *mdx*52 mice, a murine exon 52-deleted model,[30] and also measured the zeta potential of this PMO and its effect on the binding to SR-A1.

RESULTS

Endocytosis Mediates PMO Uptake into H2K-*mdx*52 Myotubes

Dystrophin deficiency has been shown to promote uptake of ASOs into myofibers, including PMOs, in *in vivo* studies,[16,31,32] presumably due to entry through unstable "leaky" plasma membranes in DMD.[33,34] However, we and others have demonstrated that PMO uptake is ATP dependent and enhanced by muscle differentiation.[16,18]

To clarify the molecular mechanism underlying PMO uptake in dystrophin-deficient muscle cells, we used the myogenic cell lines H2K-wild-type (WT) and H2K-*mdx*52. The H2K-*mdx*52 myoblasts started to fuse earlier and produced more mature myotubes than did the H2K-WT myoblasts on day 4 (Figure S1A). The expression of the muscle-specific isoform of caveolin, caveolin-3 (Cav-3), the essential component in caveolae[35] and myotube formation,[36,37] was more upregulated in H2K-*mdx*52 than in H2K-WT myotubes (Figure S1B).

On day 4, myotubes were treated for 48 h with 10 μM PMO, which targets the splicing donor site of *Dmd* exon 51 (Table 1),[38] in the absence of transfection reagent.[2] Consistent with previous *in vivo* results, only H2K-*mdx*52 myotubes showed exon-skipped bands after RT-PCR, and even 5 μM PMO induced 50% exon skipping (Figure 1A). This occurred without membrane damage, because no increase in lactate dehydrogenase release was observed (data not shown).

To investigate whether the PMO uptake in dystrophin-deficient cells was energy dependent, we incubated H2K-*mdx*52 myotubes with 1 mM NaN3 for ATP depletion. RT-PCR analysis after 48 h showed that this decreased the exon skipping by 45% (Figure 1B).

Next, to monitor PMO uptake more directly, we treated myotubes with the fluorogenic Cy5-PMO. Notably, Cy5 conjugation did not interfere with PMO-induced exon skipping (Figure 1C). When myotubes were incubated with Cy5-PMO (10 μM), H2K-WT myotubes showed no significant increase in Cy5-PMO uptake at 4 h compared with 1 h, whereas H2K-*mdx*52 myotubes showed a significant increase in uptake at 4 h (Figure 1D). H2K-*mdx*52 myotubes also showed a significantly increased uptake into their nuclei compared with H2K-WT myotubes (Figure 1E).

Next, H2K-*mdx*52 myotubes were pre-incubated with 10 mM NaN3, 30 μM chlorpromazine (CPZ) for inhibiting the clathrin-mediated pathway, 4 μg/mL filipin III (Filipin) for inhibiting the caveolin-mediated pathway, and 10 μM 5-(*N*-ethyl-*N*-isopropyl) amiloride (EIPA) for inhibiting micropinocytosis for 30 min and then supplemented with Cy5-PMO for 4 h. Consistent with the results of exon skipping, NaN3 inhibited Cy5-PMO uptake by 64%. Filipin III and EIPA inhibited Cy5-PMO uptake by approximately 50%. These results suggest that the lack of dystrophin-enhanced PMO uptake into myotubes is dependent on endocytic pathways.

Table 1. Target Exon, Target Exon-Skipping Site, Length, Sequences, and Zeta Potential in TAE Buffer at pH 7.4 of PMOs Shown in Figure 5

Name	Length (mer)	Target Exon	Target Exon-Skipping Site	Sequences	Zeta Potential (mV)
51I	25	51	internal exon	5′-CAGCCAGTCTGTAAGTTCTGTCCAA-3′	−6.0
B30	30	51	internal exon	5′-CTCCAACAGCAAAGAAGATGGCATTTCTAG-3′	−6.1
51E	25	51	internal exon	5′-ACAGCAAAGAAGATGGCATTTCTAG-3′	−6.3
23D	25	23	splice donor site	5′-GGCCAAACCTCGGCTTACCTGAAAT-3′	−10.2
51A	25	51	splice acceptor site	5′-CTGGCAGCTAGTGTTTTTGAAAGAA-3′	−12.4
53A	25	53	splice acceptor site	5′-CTGAATCTGAATTCTTTCAACTGGA-3′	−14.4
45A	25	45	splice acceptor site	5′-TGACGCTGCCCAATGCCATCCTGGA-3′	−15.0
53D	25	53	splice donor site	5′-TGACACTAACCTTGGTTTCTGTGAT-3′	−16.9
51D	25	51	splice donor site	5′-TTGTTTTATCCATACCTTCTGTTTG-3′	−18.8
55A	25	55	splice acceptor site	5′-GCAGTTGTTTCTGCTTCCGTAATCC-3′	−19.2
Poly A	25	ND	ND	5′-AAAAAAAAAAAAAAAAAAAAAAAAA-3′	−4.5
Poly T	25	ND	ND	5′-TTTTTTTTTTTTTTTTTTTTTTTTT-3′	−9.0

ND, no data.

Upregulated SR-A1 Localized in Juxtaposition with Cav-3 in Dystrophin-Deficient Myotubes Mediates PMO-Induced Exon Skipping

We then focused on the role of SR-As in receptor-mediated endocytosis of PMOs based on our report showing Pip6a-PMO uptake into C2C12 myotubes and murine skeletal muscle by SR-As.[19] Aside from SR-A2, all SR-A isoforms were expressed in both H2K-WT and -*mdx*52 myotubes, as well as in C2C12 and H2K-*mdx* myotubes, a different DMD mouse model carrying a nonsense mutation in exon 23.[19] SR-A1 expression was increased 9.5-fold in H2K-*mdx*52 myotubes compared with that in H2K-WT myotubes (Figure 2A). After fractionation of H2K-*mdx*52 myotube lysates into cytosolic and membrane fractions, most SR-A1 protein was detected as monomers near 50 kDa in the membrane fractions (Figure 2B). Confocal imaging revealed that Cav-3 was expressed along the plasma membrane in *mdx*52 myotubes (Figure 2C, left), whereas SR-A1 was present in both the cytoplasm and on the plasma membrane (Figure 2C, middle). SR-A1 was observed to localize in juxtaposition with Cav-3 but did not show co-localization, as shown in the enlarged image of the yz axis (Figure 2C, right). Concordantly, in the 3D image shown in Figure S2, Cav-3 produced a tube-shaped signal along the outline of the myotubes, and SR-A1 produced a similar pattern. Thus, these myotubes seem to express SR-A1 in the caveolae, consistent with a previous report in cell types other than myocytes.[39]

To investigate the effect of upregulated SR-A1 on PMO-induced exon skipping in *mdx*52 myotubes, we pretreated the myotubes with 10 μg/mL polyinosinic acid (poly I) as an SR-A, SR-C, SR-E, and SR-F inhibitor or fucoidan as an SR-A1/2 and SR-C1 inhibitor[33] for 1 h, and then supplemented with 5 μM PMO for 48 h in the presence of inhibitors. A lower concentration than used previously[19] was chosen to limit membrane damage. Both poly I and fucoidan partially but significantly reduced exon skipping (Figure 2D). Knockdown of each SR-A was conducted separately with small interfering RNA (siRNA). The results indicated that only SR-A1 knockdown led to a significant reduction in exon-skipping efficiency (Figure 2E). siRNA treatment of SR-A1 induced a 45% reduction in SR-A1 mRNA (Figure S3).

To examine the consequences of SR-A1 absence in PMO uptake under dystrophin-deficient conditions, we created double-knockout (DKO) mice lacking SR-A1/2 and dystrophin by crossing SR-A1/2 knockout mice with *mdx*52 mice. Satellite cells were isolated from skeletal muscles of *mdx*52 and DKO mice and differentiated into myoblasts. When these were supplemented with 5 μM Cy5-PMO for 4 h, PMO uptake was reduced by 78% in myoblasts from DKO mice compared with that in myoblasts from *mdx*52 mice (Figure 2F; Figure S4). This result is consistent with a report showing that Pip6a-PMO-induced exon skipping was less efficient in SR-A1/2 knockout than in WT mice.[19]

Furthermore, to examine the effect of SR-A1/2 overexpression on PMO uptake, pGFP-SR-A1/2 was transfected into HEK293T cells that do not express this protein.[40] Cy5-PMO uptake was promoted in these cells, which overexpressed a modified form of SR-A1/2 (Figure S5), by 4.1-fold compared with that in pGFP-transfected controls (Figure 2G, left). GFP-SR-A1/2 was distributed mainly on the plasma membrane and co-localized with Cy5-PMO (Figure 2G, right, white arrowheads), whereas pGFP-transfected cells expressed GFP only in the cytoplasm without co-localization with Cy5-PMO.

These findings suggest that PMO is taken up into dystrophin-deficient myotubes through interaction with SR-A1, which is upregulated in juxtaposition with Cav-3.

Upregulated SR-A1 in Dystrophin-Deficient Mice Promotes PMO Uptake

To reveal the *in vivo* role of SR-As in PMO uptake, we analyzed SR-A expression in murine skeletal muscle by qPCR. Consistent with the

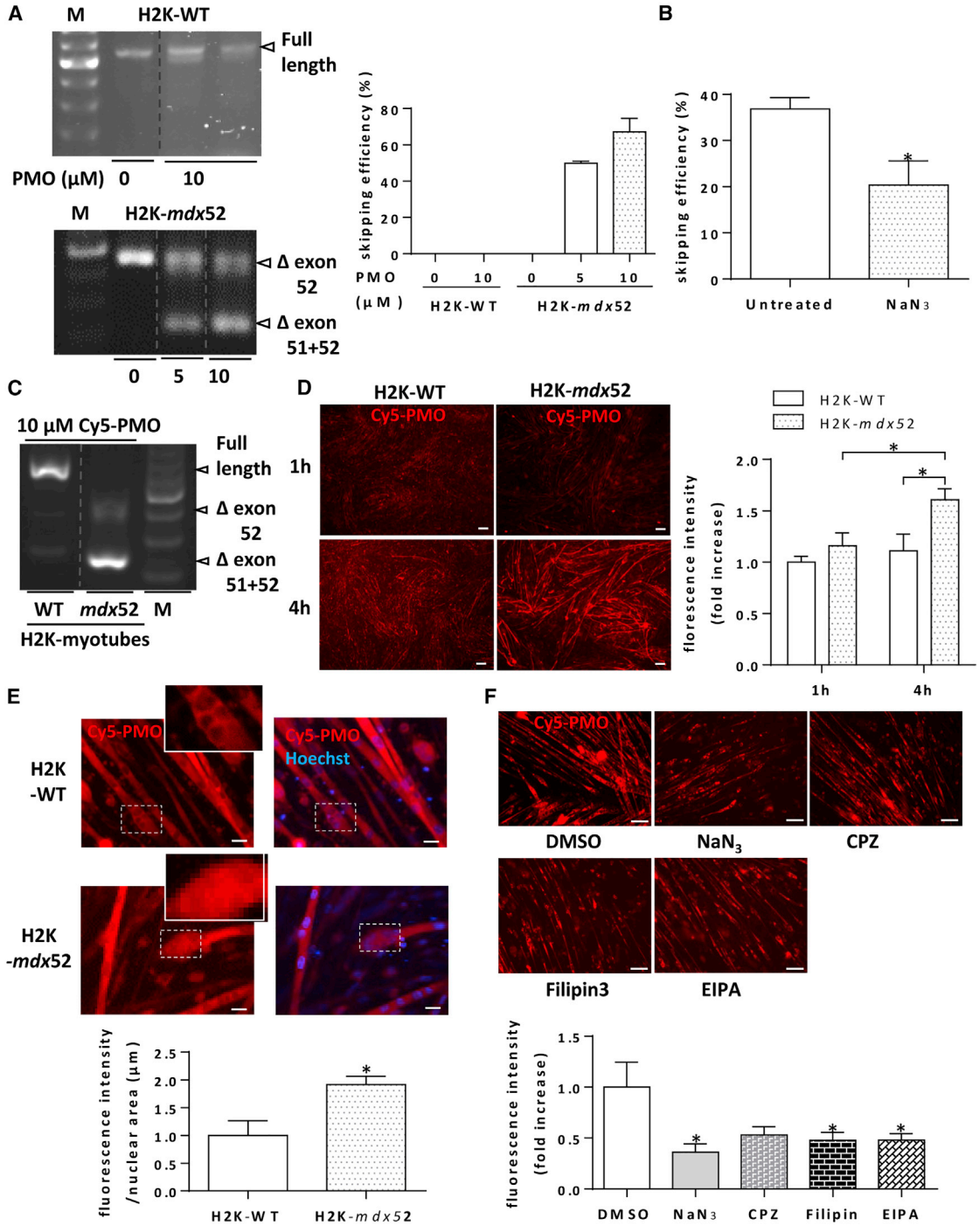

Figure 1. PMO Uptake into H2K-*mdx*52 Myotubes Is Mediated by Endocytosis

H2K-WT and *mdx*52 myoblasts were differentiated for 4 days and treated with 5 or 10 μM PMO for 48 h (A and B) or 5 or 10 μM Cy5-conjugated PMO for 1, 4 (D and E), or 48 h (C). (A) RT-PCR analysis of exon 51 skipping with cDNA from the myotubes. A representative image is shown. M, 100-bp ladder marker. The dotted line shows the division of the gel. Exon-skipping efficiency was calculated using the densitometric value of the Δexon 51 plus 52 band divided by that of all bands (Δexon 51 plus 52 and Δexon 52) (n = 3 independent experiments). (B) H2K myotubes were preincubated with 1 mM NaN3 for 1 h and then supplemented with 5 μM PMO for 48 h in the presence of NaN3. The exon-skipping efficiency was calculated from the results of RT-PCR (n = 4 independent experiments). The unpaired t test was used for statistical analysis. (C) Representative image of RT-PCR after a 48-h treatment of H2K myotubes with 10 μM Cy5-PMO. The dotted line shows the division of the gel. (D) A representative image of Cy5 fluorescence in myotubes after 5 μM Cy5-PMO treatment for 1 or 4 h. The fluorescence intensities were quantified at each time point. Two-way ANOVA was used for comparisons between

(legend continued on next page)

in vitro results, four isoforms of SR-As other than SR-A2 were expressed in the tibialis anterior (TA), gastrocnemius (GAS), and diaphragm muscles in WT and *mdx*52 mice. mRNA of SR-A1 was upregulated 17-fold in TA, 12-fold in GAS, and 6-fold in diaphragm muscles of *mdx*52 mice compared with levels in WT mice, although the differences were not significant in the TA muscles due to the large variability between individual mice ($p = 0.064$; Figure 3A). SR-A1 was mainly expressed in inflammatory lesions between myofibers but was not detected at their plasma membrane in both TA and GAS muscles from *mdx*52 mice (Figure 3B), whereas there was no signal in WT muscles, as determined by immunohistochemistry.

We confirmed that DKO mice showed almost no SR-A1 (Figure 3B) using immunohistochemistry. A dose of 75 mg/kg Cy5-PMO, which is clinically relevant, was intravenously administered to WT, *mdx*52, and DKO mice. Twenty-four hours later, the TA, GAS, diaphragm muscles, kidney, liver, and lung were isolated. Using the *in vivo* multispectral imaging system (IVIS), *mdx*52 GAS muscles showed a 2.3-fold increase in Cy5-PMO uptake compared with WT muscles, and this increase was not seen when SR-A1/2 was deleted (Figure 3C). In contrast, the uptake in TA muscles was not significantly different between the two groups, which can be explained by the large variability of SR-A1 expression levels in the muscles, as mentioned above. The Cy5 fluorescence was observed only in sections from the diaphragm (Figure 3D) and GAS muscles (Figure S6). Cy5-PMO uptake increased in the diaphragm compared with WT and DKO mice (Figure 3D). In *mdx*52 GAS muscles, Cy5-PMO uptake was limited to the cytoplasm of small, regenerating myofibers and was not seen in normal, larger myofibers (Figure S6), which was consistent with our previous findings.[16]

Cy5-PMO uptake into the kidney, liver, and lung did not change significantly among WT, *mdx*52, and DKO mice using multiple comparisons, whereas unpaired t test between *mdx*52 and DKO mice showed that there was a significant or a trend of decrease in Cy5-PMO uptake in the kidney ($p = 0.017$), liver ($p = 0.065$), and lung ($p = 0.058$) in DKO mice compared with *mdx*52 mice (Figure S7).

Finally, *Mdx*52 and DKO mice were intravenously administered 160 mg/kg body weight naked PMO, and their muscles were isolated 2 weeks later for western blotting to detect dystrophin.

Although there was no dystrophin in the TA or GAS muscles of either type of mouse, dystrophin was restored more in the diaphragms of *mdx*52 than in DKO mice (Figure 3D). The higher expression of SR-A1 in the diaphragm than in the TA and GAS muscles (Figure 3A) can explain the increased exon-skipping efficacy of PMO.

These results suggest that increased SR-A1 expression in the skeletal muscle of *mdx*52 mice mediated an increase in PMO uptake compared with that in WT mice, which agrees well with the *in vitro* results.

Upregulated SR-A1 during Muscle Regeneration Increases PMO Localization in the Nucleus

Previously, we and others reported that regenerating myofibers take up PMO more than normal myofibers.[16,17] To elucidate the role of SR-A1 in this process, *mdx*52 and DKO mice were intramuscularly injected with Cy5-PMO 1 week after intramuscular injection with $BaCl_2$ to induce muscle regeneration (Figure 4A).[41] $BaCl_2$ treatment significantly increased SR-A1 expression compared with saline control in *mdx*52 mice, but not in DKO mice (Figure 4B). Four hours after Cy5-PMO injection, the intracellular uptake into myofibers was increased in both types of mice; however, nuclear localization of Cy5-PMO in myofibers of *mdx*52 mice was more than that in DKO mice (Figure 4C). These results suggest that upregulation of SR-A1 by $BaCl_2$ during muscle regeneration increases PMO localization in the nucleus.

PMOs Have Negative Zeta Potential Based on Their Nucleobase Composition, Allowing Their Binding with SR-A1

SR-As bind to a range of negatively charged ligands with their positively charged, extracellular, collagenous domains.[27] Synthetic anionic homopolymers of RNA, such as poly G and poly I, are ligands for SR-As and derive their negative charges from phosphate groups, whereas PMO has a neutral backbone because of the replacement of phosphate with a neutral diamide.

A complex of PMO and anionic serum components, such as BSA, may have acted as a ligand for SR-As. H2K-*mdx*52 myotubes were supplemented with 5 μM PMO and incubated in culture medium with or without 1.75 mg/mL BSA or 5% horse serum (HS) for 48 h. Exon skipping was not affected by the presence of BSA or horse serum (Figure S8), suggesting that serum factors were not necessary for PMO uptake.

We previously demonstrated that the zeta potential of molecules in buffers, but not the charge of single molecules, influences the ability of molecules to bind receptors by showing that Pip6a-PMOs act as SR-A1 ligands in biomimetic conditions and at low concentrations by forming micelles with negative zeta potential.[19] Based on these findings, we hypothesized that the charge of a PMO molecule might become negative in a solvent.

multiple groups. Scale bars, 200 nm (n = 7 independent experiments). (E) Representative fluorescence images of myotubes after 5 μM Cy5-PMO treatment for 4 h, merged with nuclear staining by Hoechst (blue). Cy5 fluorescence intensity in the nuclear area (μm) was quantified using the BZ-H3CM software. The unpaired t test was used for statistical analysis. Scale bars, 20 nm (n = 4 independent experiments). (F) H2K-*mdx*52 myotubes were pre-incubated with 10 mM NaN3, 30 μM CPZ, 4 μg/mL filipin III, and 10 μM EIPA for 30 min and then supplemented with 5 μM Cy5-PMO for 4 h in the presence of each inhibitor. Representative fluorescence images of the myotubes are shown. The fluorescence intensities were quantified for each condition (n = 6 independent experiments). One-way ANOVA was used for comparisons between multiple groups. Results are presented as mean ± SE. *$p < 0.05$. N.S., not significant.

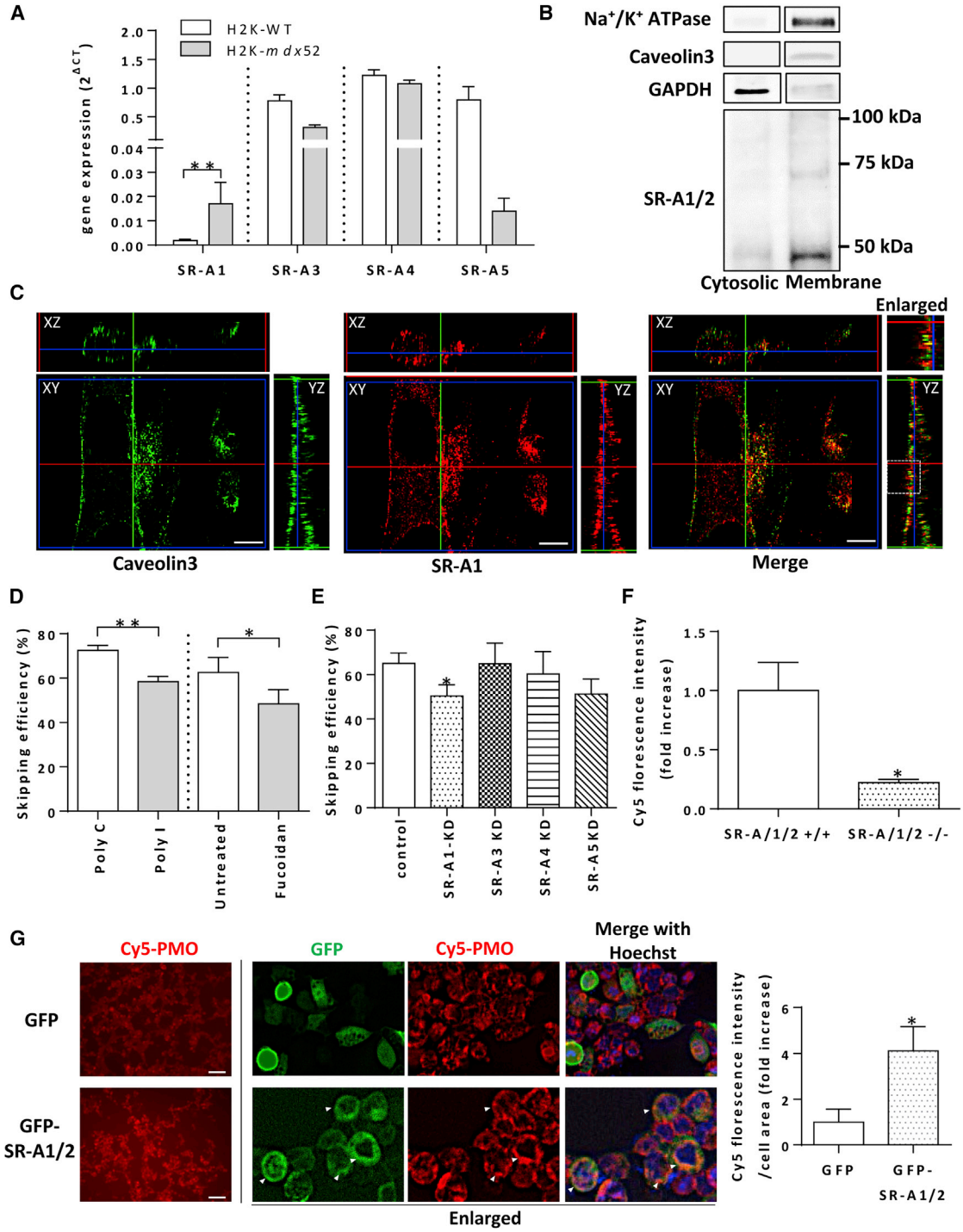

Figure 2. Role of SR-A1 in PMO Uptake into H2K-*mdx*52 Myotubes

(A) Gene expression of SR class A isoforms by qPCR using cDNA from H2K-WT and H2K-*mdx*52 myotubes 6 days after differentiation. The value of $2^{\Delta CT}$ is shown. *Abt1* was used as a housekeeping gene. The Mann-Whitney U test was used for statistical analysis (n ≥ 3 independent experiments). (B) Western blotting of SR-A1 in the lysates of H2K-*mdx52* myotubes on day 6 separated into cytosolic and membrane fractions. GAPDH was used as the control for the cytosolic fraction, and Na^+/K^+ ATPase and caveolin-3 were used as controls for the membrane fraction. Blots of each protein were derived from the same membrane. (C) Representative orthogonal sectioning of confocal images of caveolin-3 and SR-A1 in H2K-*mdx*52 myotubes on day 4 by the HyVolution method. Images of the xy, xz, and yz sections are shown. Scale bars, 10 μm. (D) H2K-*mdx*52 myotubes were pre-treated with SR inhibitors for 1 h and then supplemented with 5 μM PMO for 48 h in the presence of inhibitors. Ten micrograms per

(legend continued on next page)

Thus, we measured the zeta potential of the 10 PMOs shown in Table 1, which were randomly selected from previous reports.[2,18,19,38,42] First, the zeta potentials of PMOs 51D, 51A, 23D, 53A, and 53D were measured in PBS, OptiMEM, and tris-acetate-EDTA (TAE) (all three solvents had different conductivities) at pH 7.4 (Figure S9). Surprisingly, all five PMOs had negative zeta potentials in all conditions (Figure 5A). Furthermore, most PMOs had significantly lower zeta potentials in OptiMEM and TAE, which have lower conductivities than PBS (Figure S9). This result reflected the reduced neutralization of PMO surface charges by the fewer counter ions found in these solvents with lower conductivities. In TAE buffer, there was a significant difference between the zeta potentials of PMOs; that is, 51D had a lower potential than did 51A and 23D, and 53D had a lower one than did 23D (Figure 5A). The zeta potentials of the other five PMOs showed a range of values, with a 3.2-fold difference between the zeta potentials of 51I and 55A (Figure 5B).

To study the origin of the negative zeta potentials, we focused on the nucleobase compositions. Guanine and thymine have lower negative charges than cytosine and adenine at pH 7.4. Based on the characteristics of nucleobases, we calculated Pearson correlation coefficients between the zeta potentials and the various subtractions of base numbers or the percentages of bases for each PMO (Table 3, PMOs in Table 1 columns). The results showed a significant negative correlation between zeta potential and some of those subtractions, especially between the number of guanines plus thymines subtracted by adenines [(G + T) − A], cytosines plus adenines subtracted from thymines [T − (C + A)], and adenines subtracted from thymines (T − A) (Figure 5C; Table 3, PMOs in Table 1 columns). These results suggested that G and T contribute more than C and A to the negative zeta potential of PMOs, which is also supported by the 2-fold lower zeta potential of poly T compared with that of poly A (Figure 5D).

The negative zeta potential of PMOs mediates their interaction with the cationic surface of SR-A1. For example, the binding of 51D and 51A was tested in an affinity assay with recombinant His-tagged SR-A1. Both PMOs bound to SR-A1 are shown in Figure 5E. The equilibrium dissociation constants were calculated to be 8.61×10^{-1} μM for 51D and 6.51×10^{-1} μM for 51A.

Lower Negative Zeta Potential of PMOs Can Contribute to Increased Uptake and Exon Skipping in Myotubes

Previously, we studied the exon 51 skipping efficiency of twelve 25-mer PMOs, including 51I, 51E, 51A, and 51D, whose zeta potentials were measured in this study by intramuscular injections into the TA muscles of *mdx*52 mice, as shown in Table 2.[38] Using the sequences and the skipping efficiencies shown in Table 2, correlation coefficients were calculated (Table 3, PMOs in Table 2 columns). The results revealed a positive correlation between skipping efficiency and the number of [(G + T) − A] or [T − (C + A)]. Furthermore, other subtractions of C and/or A from G and/or T and the [G + T] percentage were positively correlated with skipping efficiency.

Next, to reveal the direct relationship among negative zeta potential, cellular uptake, and exon skipping of PMOs, H2K-*mdx*52 myotubes were supplemented with Cy5-PMOs of 51A and 51D. Four hours after treatment, 51D uptake was greater than 51A uptake both throughout the cells and in their nuclei (Figure S10A). Next, myotubes were supplemented with naked PMOs for 48 h, and their cellular uptake was detected by ELISA and exon-skipping efficiency was detected by RT-PCR. 51D (10 μM) showed increased uptake and exon-skipping efficiency compared with 51A (Figures S10B and S10C).

Therefore, the lower negative zeta potential of 51D compared with that of 51A (Figure 5A) may have contributed to the increased uptake and higher exon skipping of 51D.

As mentioned above, in the case of Pip6a-PMOs, micelle formation was essential to the retention of negative zeta potential. Our results suggested that naked PMOs could also form spontaneous micelles because of the structure of hydrophobic phosphorodiamidate linkages and hydrophilic nucleobases with negative zeta potential. Dynamic light scattering (DLS) analysis of Pip6a-PMO with the 51D sequence revealed a peak of approximately 100 nm in diameter (Figure S11A, gray line). Transmission electron microscope (TEM) visualization showed well-defined nanoparticles with diameters of approximately 50 nm (Figure S11B, upper) thought to be micelles formed by amphipathic Pip6a-PMO, as we reported previously.[19] On the other hand, PMOs with the same sequence showed a peak of approximately 3 nm in diameter by DLS analysis (Figure S11A, black line). Concordantly, TEM showed a rare, undefined form larger than 100 nm in diameter (Figure S11B, lower) thought to be the result of aggregation. Thus, PMOs did not form micelles as Pip6a-PMOs did but retained their negative zeta potential as single molecules.

DISCUSSION

In this study, we reported for the first time the *in vivo* phenomenon of dystrophin deficiency-induced PMO uptake into the cytoplasm and

microliter poly I was used as an SR class A, C, E, and F inhibitor. Ten micrograms per microliter poly C was used as a control for poly I. Ten micrograms per microliter fucoidan was used as an SR class A1/2 and C1 inhibitor. The paired t test was used for statistical analysis (n ≥ 3 independent experiments). (E) H2K-*mdx*52 myoblasts were supplemented with 5 nM siRNA for each SR-isoform for 24 h, differentiated for 4 days, and supplemented with 5 μM PMO for 48 h, followed by total RNA collection for RT-PCR detection of exon 51 skipping. The Mann-Whitney U test was used for comparisons between the control and each siRNA-treated group (n ≥ 3 independent experiments). (F) Primary satellite cell-derived myoblasts from *mdx*52 and DKO mice were supplemented with 5 μM Cy5-PMO for 4 h, and the fluorescence intensities were quantified. The unpaired t test was used for statistical analysis (n = 3 independent experiments). (G) GFP- or GFP-SR-A1/2-transfected HEK293T cells were supplemented with 5 μM Cy5-PMO for 4 h. Representative fluorescence images of the cells are shown. The fluorescence intensity of Cy5 divided by cell area was quantified in each condition. White arrowheads show co-localization of Cy5-PMO and GFP-SR-A1/2. The unpaired t test was used for statistical analysis (n = 4 independent experiments). Results are presented as mean ± SE. *$p < 0.05$; **$p < 0.01$.

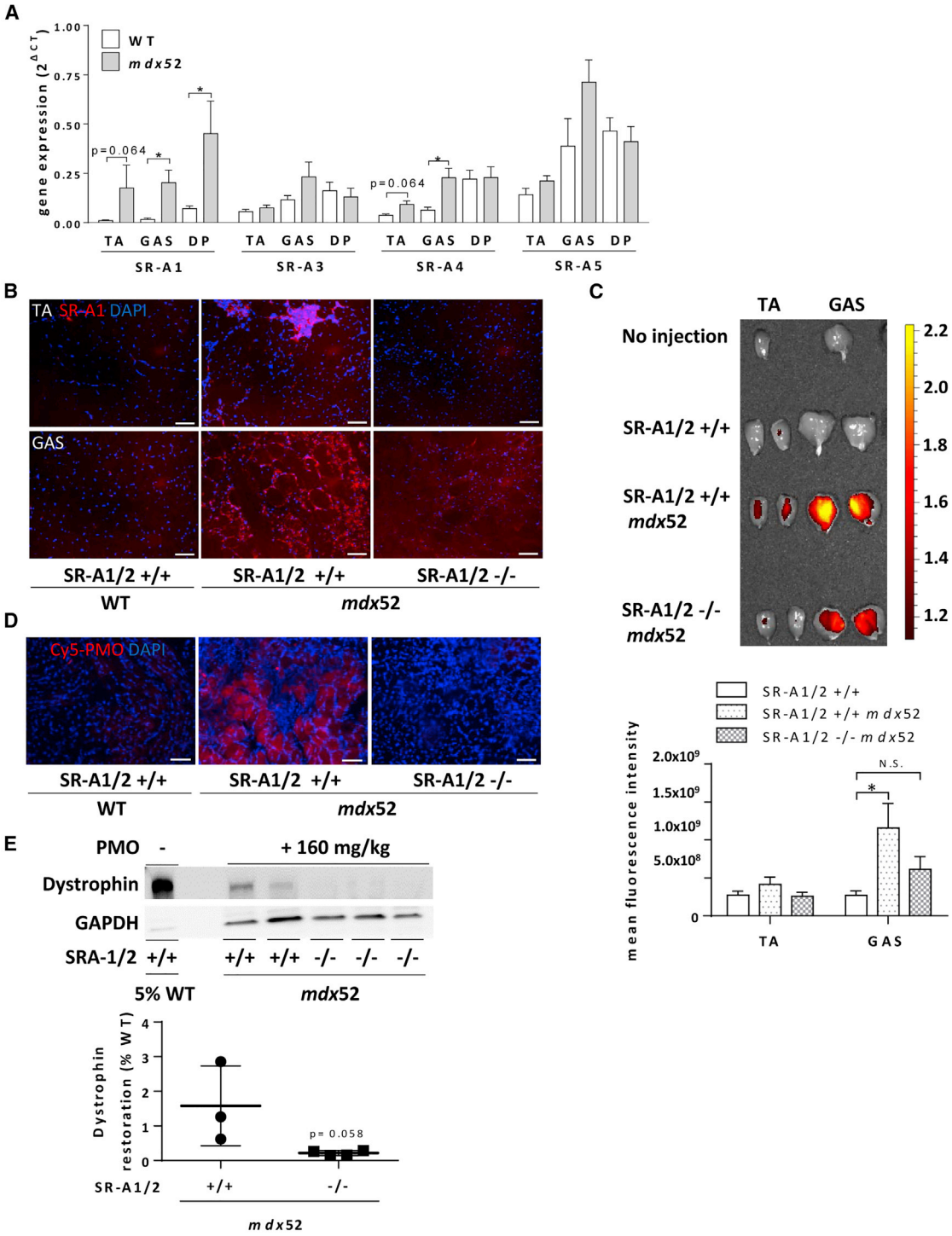

Figure 3. Upregulated SR-A1 in Dystrophin-Deficient Mice Promotes PMO Uptake

(A) Gene expression of SR class A isoforms in TA, GAS, and diaphragm (DP) muscles of 7- to 9-week-old WT and *mdx*52 mice as measured by qPCR. The Mann-Whitney U test was used for statistical analysis (n ≥ 3 independent experiments). (B) Immunohistochemistry of SR-A1 in TA and GAS muscles of 8- to 9-week-old WT, *mdx*52, and DKO mice. Scale bars, 200 μm. (C and D) Four-week-old WT, *Mdx*52, and DKO mice were intravenously injected with 75 mg/kg body weight of Cy5-PMO; 24 h later, TA, GAS, and diaphragm muscles were isolated. (C) Cy5 fluorescence in TA and GAS muscles was observed using the IVIS imaging system. Representative images are shown. Mean fluorescence intensity was quantified. One-way ANOVA was used for comparisons between multiple groups (n ≥ 6 independent experiments). (D) Cy5 fluorescence

(legend continued on next page)

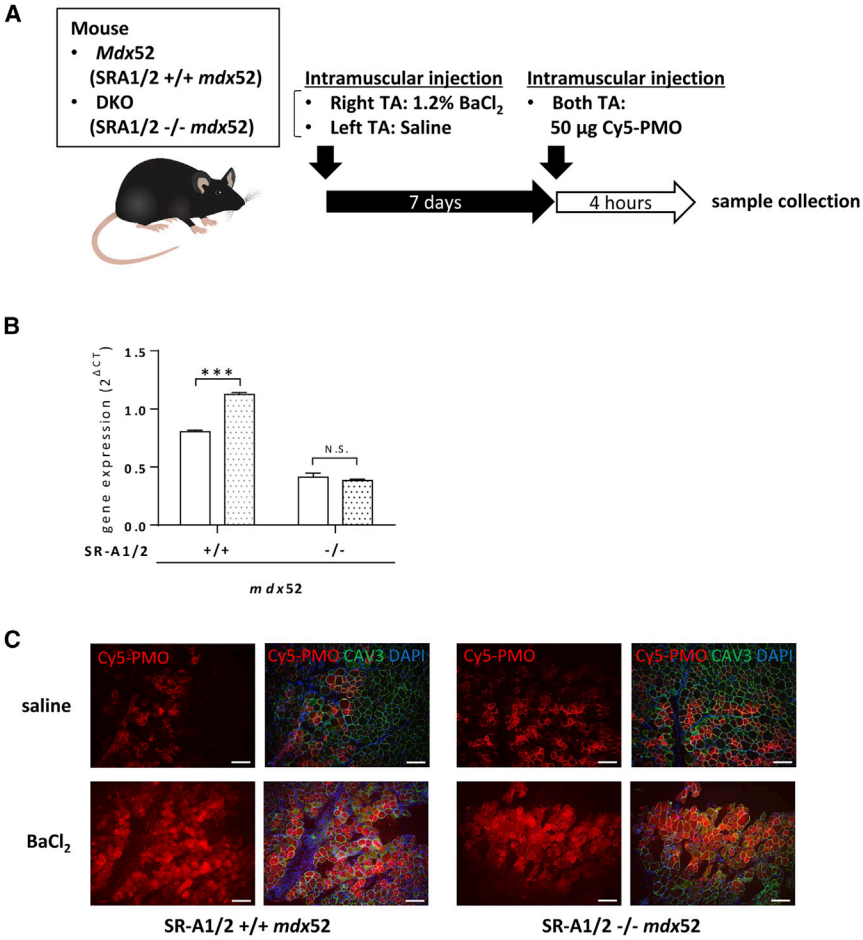

Figure 4. Upregulated SR-A1 during Muscle Regeneration Increases PMO Localization in the Nucleus

(A) Experimental model of intramuscular injection of Cy5-PMO after the induction of muscle regeneration with $BaCl_2$. *Mdx*52 and DKO mice were intramuscularly injected with 1.2% $BaCl_2$ in saline or only saline in the TA muscle of each leg. After 1 week, 50 µg of Cy5-PMO in saline was intramuscularly injected into both legs, and the muscles were collected 4 h later. (B) Gene expression of SR-A1 in TA muscles as measured by qPCR. Two-way ANOVA was used for comparisons between multiple groups ($n \geq 3$ independent experiments). (C) Frozen sections were prepared for detection of Cy5-PMO under a fluorescence microscope. Representative images of Cy5 fluorescence merged with that of caveolin-3 and nuclear staining are shown. Scale bars, 80 µm.

its exon-skipping efficiency using myogenic cell lines. Interestingly, more than half of the PMO uptake into H2K-*mdx*52 myotubes was found to be ATP dependent and mediated by endocytic pathways. Importantly, SR-A1 expression was remarkably upregulated both in H2K-*mdx*52 myotubes and in skeletal muscle of *mdx*52 mice. Reduced SR-A1 impaired PMO uptake into myotubes and myofibers, and resulted in reduced PMO-induced exon skipping. Furthermore, PMOs had negative zeta potential that depended on their nucleobase compositions despite their neutral backbones, which enable their interaction with SR-A1.

To date, changes in dystrophin-deficient muscle membrane permeability were thought to facilitate the entry of PMO into myofibers; this so-called leaky membrane hypothesis was the favored explanation for PMO uptake and was based on *in vivo* animal studies[16,31,32] and clinical evidence.[43] Considering the role of dystrophin as a membrane stabilizer that prevents contraction-induced damage, its deficiency induces the energy-independent, nonspecific uptake of extracellular PMO through dystrophin-deficient plasma membranes. However, our findings strongly support that PMO uptake is regulated by SR-A1-mediated endocytosis and not by a nonspecific pathway.

We focused on the role of SR-As in receptor-mediated endocytosis of PMOs based on reports showing Pip6a-PMO uptake into C2C12 myotubes and murine skeletal muscle mediated by SR-As.[19] Among the SR-As, only SR-A1 expression and protein production were remarkably upregulated by dystrophin deficiency, and exon-skipping efficiency was reduced partially by SR inhibitors or after 50% SR-A1 knockdown at the mRNA level. SR-A1-deleted primary myoblasts from DKO mice showed a 78% reduction in Cy5-PMO uptake compared with that in myoblasts from *mdx*52 mice.

On the plasma membranes of H2K-*mdx*52 myotubes, SR-A1 localized in juxtaposition with Cav-3 (Figures 2B and 2C; Figure S2). Cav-3 and caveolae formation are upregulated in patients with DMD, *mdx* mice, and *mdx*52 mice,[35,44,45] and also induce myotube formation.[36,37] In addition, SR-A1 expression increased significantly throughout the course of differentiation in both C2C12 and H2K-*mdx* cells.[19] Taken together, these findings suggest that Cav-3 upregulation due to dystrophin deficiency (Figure S1B) may enhance SR-A1 expression in DMD and lead to increased PMO uptake in

was observed in the sections of diaphragm muscles. Representative images of Cy5 fluorescence with DAPI are shown. Scale bars, 80 nm. (E) Four- to five-week-old *mdx*52 and DKO mice were intravenously injected with 160 mg/kg body weight of PMO; 2 weeks later, muscles were isolated, and their lysates were used for western blotting to detect dystrophin restoration. A representative image of western blotting of diaphragm lysates is shown. Thirty micrograms of total protein was loaded relative to 5% (1.5 µg of protein) WT control and normalized to the GAPDH loading control. The graph shows the quantified data ($n \geq 3$ independent experiments). Results are presented as mean ± SE. *$p < 0.05$; **$p < 0.01$. N.S., not significant.

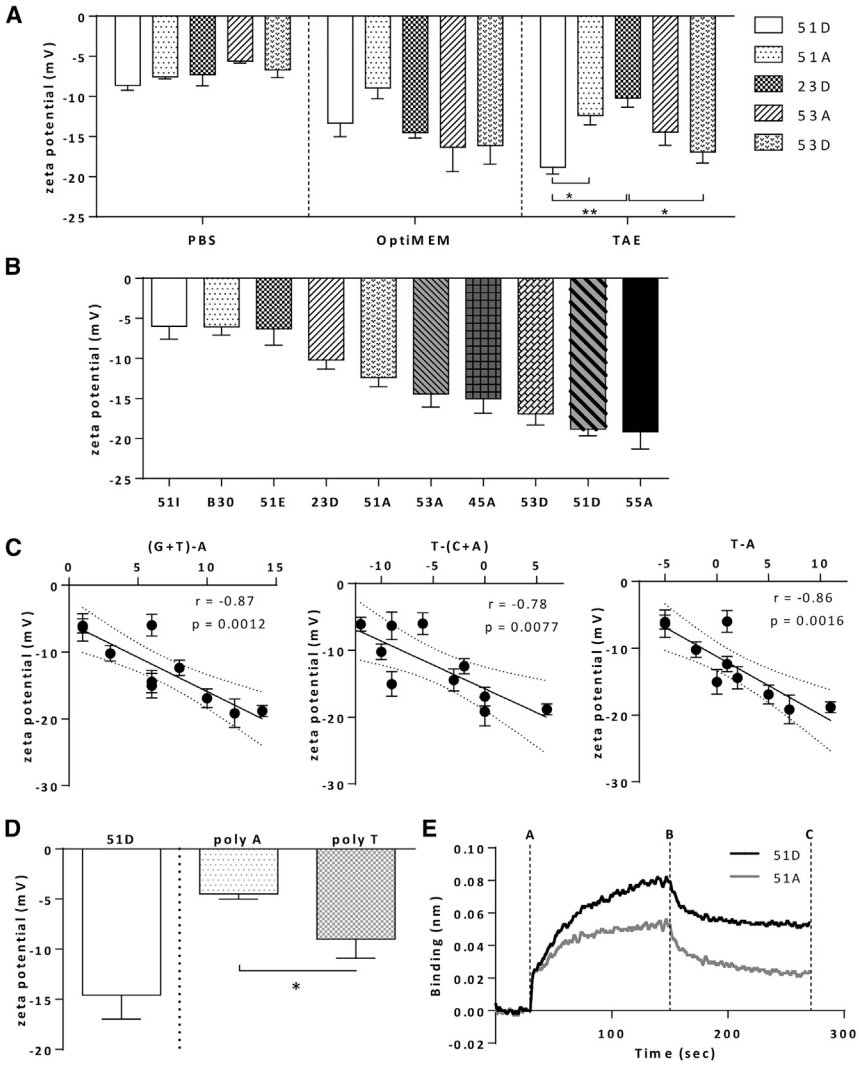

Figure 5. PMOs with Negative Zeta Potential Bind to SR-A1

(A) The zeta potentials of 50 μM PMOs, the sequences of which are shown in Table 1, were measured in PBS, OptiMEM, and TAE at pH 7.4. One-way ANOVA was used for comparisons between multiple groups in each solvent ($n \geq 3$ independent experiments). (B) Zeta potentials of all 10 PMOs in Table 1 measured in TAE at pH 7.4. The conductivity of each buffer is shown in Figure S9, and the sequence of each PMO is shown in Table 1. (C) The correlation between the zeta potential of PMOs in TAE buffer and the number of adenines subtracted from guanines plus thymines [(G + T) − A], cytosines plus adenines subtracted from thymines [T − (C+A)], and adenines subtracted from thymines (T − A). Pearson correlation coefficients and p values are indicated. (D) The zeta potentials of 50 μM PMOs, 51D, and poly A or poly T were measured in TAE at pH 7.4. The unpaired t test was used for statistical analysis ($n \geq 4$ independent experiments). (E) PMOs (51D and 51A) were tested in a binding affinity assay with an N-terminal polyhistidine (His)-tagged recombinant SR-A1 by bio-layer interferometry. The anti-His tag biosensor was bound to SR-A1 and incubated with 1 μM of each PMO. During PMO incubation, the instrument recorded the kinetics of binding of PMO. The area between lines A and B corresponds to the association phase, and the area between lines B and C corresponds to the dissociation phase. Results are presented as means ± SE. *$p < 0.05$; **$p < 0.01$; ***$p < 0.001$.

differentiating or regenerating processes *in vivo* and *in vitro*[16,17,28] mediated by caveolin (caveolae)-dependent endocytosis via SR-A1 (Figure 1F). There may be other pathways of PMO uptake, such as endocytosis by other classes of SRs localizing in caveolae, such as SR-B3 (CD36), a fatty acid transporter in skeletal muscle[46]; macropinocytosis, as shown in Figure 1F[47]; or heteromultimeric receptor complexes (signalosomes) comprising SRs and other coreceptors.[20]

SR-A1 was expressed at the plasma membrane only in cells in culture, but not in myofibers *in vivo*. It is possible that immortalization of H2K-myoblasts promotes SR-A1 expression in these cells, whereas *in vivo* factors, such as inflammatory status,[48] could influence the downregulation of SR-A1 at the plasma membrane. On the other hand, SR-A1 was detected only in inflammatory lesions of the interstitial space in skeletal muscles in which inflammatory cells, including macrophages, are generally observed.[17] Given that SR-A1 is known to be expressed in macrophages,[20] which could mediate PMO uptake as reported previously,[17] it is possible that the PMO uptake into macrophages mediated by SR-A1 and the subsequent extracellular release eventually led to PMO uptake into myofibers. Future studies using muscle-specific SR-A1 knockout mice will clarify the role of SR-A1 in PMO uptake.

Our first study of the molecular mechanisms of uptake of PMOs with neutral backbones was different from previous studies of phosphorothioate (PS)-ASOs with negatively charged backbones. A previous study on PS-ASO uptake in SR-A1/2 knockout and WT mice showed that SR-A1 does not play a major role in PS-ASO uptake, even in tissues in which SR-A1 expression is high.[49] Stabilin-1 and stabilin-2, categorized as SR-Hs, are likely to be more important as specific receptors for the cellular internalization of PS-ASOs in the liver.[50] Interestingly, *in vitro* stabilin-2-mediated internalization of PS-ASO in cells did not compete with PMO uptake. Taken together, these results suggest that the varying negative zeta potentials resulting from PS modifications to PS-ASOs and nucleobases in PMOs can differentially affect binding affinity to SRs, as represented by their large differences in plasma protein binding characteristics, tissue distribution, and half-lives.[51]

In addition, cell-penetrating peptide modification can change the cellular uptake pathway of PMO. A previous study showed that Pip6a-PMO was taken up by H2K-*mdx* myotubes only by a caveolin-dependent pathway, and not by micropinocytosis,[28] which was

Table 2. Target Exon-Skipping Site, Sequence, and Exon-Skipping Efficiency for PMOs

Name	Target Exon 51 Skipping Site	Sequences	Skipping Efficiency (%)
51A	splice acceptor site	5′-CTGGCAGCTAGTGTTTTTGAAAGAA-3′	31
51B	internal exon	5′-TCACCCACCATCACTCTCTGTGATT-3′	5
51C	internal exon	5′-ATGTCTTCCAGATCACCCACCATCA-3′	12
51D	splice donor site	5′-TTGTTTTATCCATACCTTCTGTTTG-3′	56
51E	internal exon	5′-ACAGCAAAGAAGATGGCATTTCTAG-3′	39
51F	internal exon	5′-TCACTAGAGTAACAGTCTGACTGGC-3′	15
51G	internal exon	5′-CCTTAGTAACCACAGATTGTGTCAC-3′	22
51H	internal exon	5′-TTCTAGTTTGGAGATGACAGTTTCC-3′	42
51I	internal exon	5′-CAGCCAGTCTGTAAGTTCTGTCCAA-3′	45
51J	internal exon	5′-AGAGACAGCCAGTCTGTAAGTTCTG-3′	29
51K	internal exon	5′-CAAGCAGAGACAGCCAGTCTGTAAG-3′	7
51L	internal exon	5′-TCACTCTCTGTGATTTTATAACTCG-3′	18

The information was adapted from *Molecular Therapy*[38] with permission.

different from our results showing the involvement of both pathways in naked PMO uptake. Our study showed that naked PMO did not form micelles as Pip6a-PMO did, which is thought to be effective for SR-A1-mediated endocytosis based on the particle-wrapping model.[19] This could lead to partial utilization of macropinocytosis in naked PMO uptake independent of SR-A1 because this pathway does not rely on special protein coatings or concentrated receptors on the membrane surface, unlike other endocytotic pathways.[52]

SR-As recognize negatively charged compounds directly or indirectly by association with anionic serum proteins.[53,54] Our results suggest that serum factors and BSA are not necessary for PMO uptake (Figure S8), which was consistent with the poor plasma protein-binding characteristics of PMO.[51] Unexpectedly, 10 PMOs randomly selected from previous studies had negative zeta potentials (Figure 5B), which allowed their physical binding to recombinant SR-A1 (Figure 5E). We demonstrated that this difference originated partially from their nucleobase compositions by correlation analyses focused on bases with high pKa values (G and T) and low pKa values (C and A) (Figure 5C) and on poly T in PMO backbones producing lower negative zeta potential than does poly A (Figure 5D). This characteristic is thought to be specific to ASOs with charge-neutral backbones, such as PMOs and peptide nucleic acids (PNAs), because 2′-O-substitution and PS linkages in other ASOs have much more influence on their negative charges than do their nucleobases.[55]

It has been reported that the efficiency of exon skipping varies markedly between different target sequences depending on interactions between ASOs and a complex system comprising the splicing apparatus and regulatory factors, nascent pre-mRNA, and the rest of the cellular environment.[56] Our study proposes cellular uptake of ASOs based on their sequences as novel regulatory factors occurring in the first step of interaction between ASOs and target cells, in addition to the above factors (Figure S10; Table 3). For further evaluation of the relationship between zeta potential, cellular uptake, and exon-skipping efficiency, it will be necessary to analyze a larger set of PMOs with different sequences as shown in Table 1 or 2, instead of the two used in this study.

SR-A1 expression was upregulated in diaphragm muscles compared with those in TA and GAS muscles, and PMO was taken up into a wider range of myofibers in diaphragm muscles than in the other muscles and induced detectable exon skipping by single PMO administration, which was not observed in the other muscles. Together with the result of upregulated PMO uptake in GFP-SR-A1/2-overexpressed HEK293T cells, these results suggest that tissues with high SR-A1 expression can be good targets for the treatment of DMD using PMO, which can be applied to tissue targeting in other neuromuscular diseases or genetic disorders. The role of SR-A1 in PMO uptake in non-muscle tissues was supported by the result that deletion of SR-A1 significantly reduced PMO uptake into the kidney, liver, and lung.

In conclusion, this is the first study to demonstrate that naked PMOs can have negative zeta potentials and can be taken up into dystrophin-deficient myotubes and myofibers by upregulated SR-A1-mediated endocytosis. Notably, it explains dystrophin deficiency-induced exon skipping, which had been explained mainly by dystrophin deficiency-induced plasma membrane leakiness. The development of an SR-A1-targeting drug delivery system could lead to highly efficient exon-skipping therapies for DMD or other neuromuscular diseases.

MATERIALS AND METHODS

Animals

Mice with exon 52-deficient X chromosome-linked muscular dystrophy (*mdx*52 mice) were provided by the Riken BioResource Center (Wako Pure Chemical Corporation, Tokyo, Japan) through the National Bio-Resource Project of the MEXT, Japan.[57] Mice genetically deficient in SR-A1/2 (SR-A1/2$^{-/-}$), generated by disrupting exon 4 of the SR-A gene essential to the formation of functional

Table 3. Pearson Correlation Coefficients and p Values of Comparisons between the Numbers or Percentages of Indicated Nucleobases in Each PMO and Its Zeta Potential or Skipping Efficiency

	Pearson Correlation Coefficients			
	PMOs in Table 1		PMOs in Table 2	
	r	p Value	r	p Value
(G+T) − (C+A)	−0.6951	0.0257*	0.7077	0.01*
(G+T) − C	−0.4581	0.183	0.7059	0.0103*
(G+T) − A	−0.8671	0.0012**	0.6121	0.0344*
G − (C+A)	−0.649	0.0423*	0.6156	0.0331*
T − (C+A)	−0.7805	0.0077**	0.6525	0.0214*
G − C	0.2071	0.5659	0.4255	0.1679
T − C	−0.5447	0.1035	0.7206	0.0082**
G − A	−0.7475	0.013*	0.5202	0.0829
T − A	−0.8557	0.0016**	0.4568	0.1354
G + T (%)	−0.7581	0.0111*	0.7077	0.01*
G + C (%)	0.1485	0.6821	−0.6283	0.0287*
G (%)	0.361	0.3055	0.1794	0.5769
T (%)	−0.7538	0.0118*	0.5264	0.0787

Regarding the calculation using nucleobase composition, for example, 51D has 3 guanines (G), 14 thymines (T), 5 cytosines (C), and 3 adenines (A), as shown in Table 1 or 2. Thus, [(G + T) − (C + A)] is calculated to be 9 for 51D.
*$p < 0.05$.
**$p < 0.01$.

trimeric receptors,[58] were purchased from Charles River Laboratories (JAX stock 006096; Kanagawa, Japan) and crossed with *mdx*52 mice to produce SR-A1/2$^{-/-}$ *mdx*52 DKO mice. Age-matched male *mdx*52, DKO, and C57BL/6J WT mice (Charles River Laboratories) were used in this study. The mice were allowed *ad libitum* access to food and drinking water. The Experimental Animal Care and Use Committee of the National Institute of Neuroscience, National Center of Neurology and Psychiatry, Japan, approved all experimental protocols in this study.

PMOs

PMOs of different sequences listed in Table 1 were purchased from Gene Tools (Philomath, OR, USA). Cy5-conjugated PMO and Pip6a-PMO with sequence 51D (Pip6a, RXRRBRRXR YQFLI RXRBRXRB, X, 6-aminohexanoic acid; B, β-alanine)[29] were synthesized by Nippon Shinyaku (Kyoto, Japan).

H2K-*mdx*52 Myoblasts

H-2Kb-tsA58 × *mdx*52/*mdx*52 F1 male mice yielded dystrophin-deficient H2K-*mdx*52 myoblasts.[29] H2K-WT and H2K-*mdx*52 myoblasts were seeded onto gelatin-coated 24-well plates at a density of 5×10^4 cells/well and grown at 33°C in DMEM with GlutaMAX, interferon-γ (IFN-γ) at a concentration of 20 U/mL, and 20% (v/v) fetal bovine serum. After treatment, cells were differentiated into myotubes in DMEM with GlutaMAX containing 5% (v/v) horse serum (HS) at 37°C. Four days after the initiation of differentiation, the myotubes were used for experiments.

PMO Supplementation

Myotubes were supplemented with 5 or 10 μM PMOs in differentiation medium without any transfection reagents for 48 h for exon-skipping analysis.

RNA Isolation and RT-PCR

Total RNA was extracted from cells or frozen murine muscle sections using TRIzol (Invitrogen, Carlsbad, CA, USA). One hundred nanograms of total RNA template was used for RT-PCR with a High-Capacity cDNA Reverse Transcription Kit (Thermo Fisher Scientific, Waltham, MA, USA) according to the manufacturer's instructions. For one RT-PCR, 1 μL of cDNA template was mixed with 14.3 μL of water, 0.5 μL of 10 μM forward primer, 0.5 μL of 10 μM reverse primer, 1.6 μL of 2.5 mM dinucleotide triphosphates (dNTPs), 2 μL 10× Ex Taq Buffer, and 0.1 μL Ex Taq horse serum from the Ex Taq Hot Start Version kit (Takara Bio, Shiga, Japan). The primer sequences used were Ex50F 5′-GAGTGGGAGGCTGTAAACCA-3′ and Ex53R 5′-ACCTGTTCGGCTTCTTCCTT-3′ for amplification of cDNA from exons 50–53. The cycling conditions were 95°C for 4 min, 35 cycles of 94°C for 30 s, 61°C for 30 s, 72°C for 30 s, and finally 72°C for 7 min. The intensity of PCR bands was analyzed using the ImageJ software (https://imagej.nih.gov/ij/; NIH, Bethesda, MD, USA), and skipping efficiency was calculated by dividing the densitometric value of the Δexon 51 plus 52 band with that of all bands (Δexon 51 plus 52 and Δexon 52).

qPCR

TaqMan probes were purchased from Thermo Fisher Scientific. cDNA synthesized from 1 μg of total RNA was used for qRT-PCR using predesigned fluorescein amidite (FAM-MGB)-conjugated TaqMan probes for target genes, and Abt1-VIC-PL was used as an internal housekeeping reference.

Fluorescent-Conjugated PMO Uptake Study

In an *in vitro* study, cells were supplemented with 5 μM Cy5-PMO for 1 and 4 h. Three images from each well were randomly taken at 20× magnification with a BZ-9000 fluorescence microscope (Keyence, Osaka, Japan), and the fluorescence intensity was quantified by ImageJ. The background was subtracted from the image of untransfected cells. For HEK293T cells, the fluorescence intensity was divided by cell area calculated by the BZ-H3CM software (Keyence). The averaged intensity from three images was used for comparison. Nuclear fluorescence intensity was quantified by the BZ-H3CM software.

Fractionation of Cell Lysates

All reagents were acquired from G-Biosciences (St. Louis, MO, USA). Myotube monolayers were lysed and fractionated into cytosolic (soluble) and membrane (insoluble) fractions with a FOCUS Global Fractionation Kit according to the manufacturer's protocol. Protein concentration was determined using a Non-interfering Protein Assay Kit.

Preparation of Muscle Lysates

Muscle lysates from mice were prepared according to our protocol.[30] In brief, 20 × 12 μm muscle cryosections were homogenized in

100 μL of radioimmunoprecipitation assay (RIPA) buffer with Complete Mini Protease Inhibitor Cocktail (Roche, Basel, Switzerland), heated at 95°C for 5 min, and centrifuged at 16,500 × *g* for 15 min. The supernatant containing the lysates was then collected. The protein concentration was determined with a BCA Protein Assay Kit (Thermo Fisher Scientific) according to the manufacturer's protocol.

Western Blotting

Equal amounts of the lysates were denatured in Laemmli sample buffer (Bio-Rad, Hercules, CA, USA) with 2-mercaptoethanol at 55°C (for SR-A1/2) or 70°C (for dystrophin) for 10 min, and then separated by SDS-PAGE and transferred to polyvinylidene difluoride (PVDF) membranes. The PVDF membranes were blocked with Tris-buffered saline containing 0.1% Tween 20 and 5% BSA (for SR-A1/2) or 5% milk (for dystrophin). The membranes were incubated overnight with anti-SR-A1/MSR (R&D Systems, Minneapolis, MN, USA), anti-dystrophin (NCL-DYS1; Leica Microsystems, Tokyo, Japan), anti-GAPDH (Santa Cruz Biotechnology, Dallas, TX, USA), anti-Cav-3 (BD Biosciences, Franklin Lakes, NJ, USA), Na,K-ATPase (Cell Signaling Technologies, Danvers, MA, USA), or anti-α-actinin (Sigma-Aldrich, St Louis, MO, USA), followed by incubation with goat (Invitrogen), rabbit, or mouse (GE Healthcare, Little Chalfont, UK) secondary antibodies conjugated to horseradish peroxidase. The signals were detected by ECL Prime Western Blotting Detection Reagent (GE Healthcare).

Immunocytochemistry

An eight-well chamber slide (Iwaki, Shizuoka, Japan) was coated with growth factor-reduced Matrigel (Corning, Corning, NY, USA), and H2K-*mdx*52 myoblasts were seeded on the slide with growth media. After 2 days, they were differentiated using 5% horse serum differentiation media. After 4 days, cells were fixed with methanol at −20°C for 10 min. After being washed with PBS, cells were permeabilized with 0.1% Triton X-100 in PBS for 10 min and then blocked with Mouse Blocking Reagent (Vector Laboratories, Burlingame, CA, USA) for 1 h at 20°C–25°C, followed by incubation with anti-SR-A1/MSR (1:400; R&D Systems) and anti-Cav-3 (1:200; BD Biosciences) for 1 h at 20°C–25°C. After being washed with PBS, cells were probed with Alexa Fluor 647 (1:200, for SR-A1) and Alexa Fluor 488 (1:200, Cav-3) secondary antibodies (Invitrogen) for 1 h at 20°C–25°C. After being washed with PBS, cells were mounted using mounting medium with DAPI (Vector Laboratories).

Immunohistochemistry

Eight-micrometer-thick cryosections on glass slides were fixed with acetone at −20°C (for SR-A1) or 4% paraformaldehyde at room temperature (for Cav-3) for 10 min, permeabilized with 0.1% Triton X-100 in PBS for 10 min (only for SR-A1), and blocked with 5% horse serum in PBS at 37°C for 15 min (for SR-A1) or Mouse on Mouse Blocking Reagent at room temperature for 1 h (for Cav-3). The sections were incubated with anti-SR-A1/MSR (1:100) or anti- Cav-3 (1:200) at 20°C–25°C for 1 h, washed with PBS, and probed with Alexa Fluor 647 (1:200, for SR-A1) or Alexa Fluor 488 secondary antibodies (1:200, for Cav-3) at 20°C–25°C for 1 h. After being washed with PBS, the sections were mounted using mounting medium with DAPI.

Confocal Imaging

Images were acquired with a Leica TCS SP5 confocal system equipped with a hybrid detector (HyD; Leica Microsystems) using the LAS AF software. Images of myotubes were acquired using a 63×/1.4 oil immersion objective lens at a 1,024 × 1,024-pixel resolution and with a z-step of 0.15 μm. The scan speed was 100 Hz. The photon-counting mode of the hybrid detector was used. The zoom factor and frame accumulation used were 5.6 and 6, respectively. The acquired images were deconvoluted with Leica Application Suite X (LAS X).

Endocytosis Inhibitor Treatment

All inhibitors were acquired from Sigma-Aldrich. For exon-skipping analysis, H2K-*mdx*52 myotubes were pre-incubated in differentiation medium with 1 mM NaN_3 for 1 h and then supplemented with 5 μM PMO for 48 h in the presence of NaN_3. For the study of PMO uptake, the myotubes were pre-incubated in differentiation medium with 10 mM NaN_3, 30 μM CPZ, 4 μg/mL filipin III, and 10 μM EIPA for 30 min, and then supplemented with 5 μM Cy5-PMO for 4 h in the presence of each inhibitor.

SR Inhibitor Treatment

For exon-skipping analysis, H2K-*mdx*52 myotubes were pre-treated with SR inhibitors from Sigma-Aldrich for 1 h and then supplemented with 5 μM PMO for 48 h in the presence of the inhibitors. Ten micrograms per milliliter of fucoidan, poly I, and polycytidylic acid (poly C) was used as an SR-A1/2 and SR-C1 inhibitor;[33] an SR-A, SR-C, SR-E, and SR-F inhibitor; and as a negative control for poly I, respectively.

siRNA Knockdown of SRs

H2K-*mdx*52 myoblasts were seeded at a density of 5×10^4 cells per well in 24-well plates, incubated for 24 h, and then supplemented with 5 nM siRNA for each SR-A for 24 h using Lipofectamine RNA iMAX Reagent (Thermo Fisher Scientific) according to the manufacturer's protocol. To evaluate knockdown efficiency, we collected total RNA from the myoblasts for qPCR. For PMO treatment, the myoblasts were differentiated for 4 days and supplemented with 5 μM PMO for 48 h.

Primary Satellite Cell-Derived Myoblasts

EDL muscles from *mdx*52 and DKO mice were isolated and dissociated by digestion using type 1 collagenase as previously described.[59] Satellite cells were cultured and differentiated into proliferating myoblasts in a growth medium (DMEM with GlutaMAX, 20% FBS, 1% chicken embryo extract, 10 ng/mL basic fibroblast growth factor; Cell Signaling Technologies), and 1% penicillin-streptomycin at 37°C under 5% CO_2).

Plasmid Transfection into HEK293T Cells

pCMV6-C-GFP and -GFP-SR-A1/2 were purchased from OriGene Technologies (Rockville, MD, USA). Each 2.5-μg plasmid was

transfected into HEK293T cells at a density of 2×10^4 cells/well in a 96-well plate with Lipofectamine LTX Reagent (Thermo Fisher Scientific) for 24 h. The cells were then supplied with 5 μM Cy5-PMO for 4 h, and Cy5 fluorescence was observed with a fluorescence microscope.

Intravenous Administration of PMO into Mice

Four- to five-week-old *mdx*52 and DKO mice were administered 160 mg/kg body weight PMO through their tail veins; 2 weeks later, their muscles were isolated and muscle lysates were used in western blotting to detect dystrophin. Thirty micrograms of total protein was loaded relative to 5% (1.5 μg protein) WT control and normalized to the GAPDH loading control.

Intramuscular Administration of PMO into Mice

Seven- to eight-week-old *mdx*52 and DKO mice were intramuscularly injected with 1.2% $BaCl_2$ in saline or only saline in the TA muscle of each leg. After 1 week, 50 μg of Cy5-PMO in saline was intramuscularly injected into both legs; the muscles were collected 4 h later and then used for qPCR analysis or immunohistochemistry.

PMO Uptake into Skeletal Muscle

Seventy-five milligrams per kilogram body weight Cy5-PMO was diluted in 100 μL of saline and intravenously administered into 4-week-old male WT, *mdx*52, and DKO mice. After 24 h, the mice were sacrificed by cervical dislocation, and their TA and GAS muscles were isolated for imaging and quantification with the IVIS imaging system (Summit Pharmaceuticals International, Tokyo, Japan), or 12-μm cryosections were imaged by fluorescence microscopy.

Conductivity, DLS, and Zeta Potential Measurement

Conductivity, DLS, and zeta potential measurements were performed on a Zetasizer Nano ZS (Malvern Panalytical, Worcestershire, UK) using 20 or 50 μL of 50 μM PMO in quartz cells or capillary cells in the indicated buffers.

ELISA for PMO Uptake

ELISA was performed based on previous protocols.[12,60] Protein extracts from untreated, 51D-treated, and 51A-treated cells were diluted and used for ELISA. PMO standards of known concentration were also included. Samples were hybridized to probes (Integrated DNA Technologies, Skokie, IL, USA) for 51D or 51A as previously described.[60] Both probes were labeled at the 5′ and 3′ ends with digoxigenin and biotin, respectively, and had the first and last seven bases phosphorothioated. Samples were processed as previously described.[60] Absorbances at 444 nm excitation and 555 nm emission (cutoff 530 nm) were obtained with a plate reader (Molecular Devices, San Jose, CA, USA). PMO uptake amounts were calculated using standard curve equations ($R^2 \geq 0.992$) derived from PMO standard data.

TEM

Visualization of negative staining was conducted with 800 μM Pip6a-PMO and PMO by the Hanaichi UltraStructure Research Institute (Aichi, Japan) using a JEOL JEM-1200EX TEM (JEOL, Peabody, MA, USA).

Bio-layer Interferometry Assays

Bio-layer interferometry (BLI) assays between PMO and SR-A1 were conducted using a BLItz system (ForteBio, Fremont, CA, USA). Before starting the experiment, the anti-N-terminal polyhistidine (His) biosensor was equilibrated in 10 mM Tris and 150 mM NaCl for 10 min. Next, the biosensor was incubated with 10 μg/mL His-tagged SR-A1 recombinant protein (R&D Systems) in this buffer for 2 min, washed for 30 s, and then 1 μM PMO was incubated with the biosensor for another 4 min while the instrument recorded the kinetic binding ability of the PMOs; the equilibrium dissociation constant was calculated with BLItz Pro 1.2. 1.5 software (ForteBio).

Lactate Dehydrogenase Assays

Lactate dehydrogenase activity in the conditioned medium from H2K-*mdx*52 myotubes after treatment with reagents was measured using a cytotoxicity detection kit (Roche) following the manufacturer's instructions.

Statistical Analysis

Data are shown as mean ± SE. A two-tailed t test or Mann-Whitney U test was used for comparisons between two groups. For multiple comparisons, data were analyzed using a one-way or two-way ANOVA followed by the Bonferroni correction. The Pearson correlation coefficient (r) and its square (r^2) were used for correlation analysis. $p < 0.05$ was considered to be significant.

SUPPLEMENTAL INFORMATION

Supplemental Information includes 11 figures and can be found with this article online at https://doi.org/10.1016/j.omtn.2019.01.008.

AUTHOR CONTRIBUTIONS

Conceptualization, S.M. and Y.A.; Methodology, S.M. and Y.A.; Investigation, S.M., Y.M., M.K.T., K.R.Q.L., and Y.H.; Writing – Original Draft, S.M.; Writing – Review & Editing, S.M. and Y.A.; Funding Acquisition, Y.A. and S.T.; Resources, F.S. and T.Y.; Supervision, Y.A.

CONFLICTS OF INTEREST

The National Center of Neurology and Psychiatry is now developing NS-065/NCNP-01, an exon 53-skipping drug in DMD with Nippon Shinyaku Co., Ltd.

ACKNOWLEDGMENTS

This work was supported by the Japan Society for the Promotion of Science Grant-in-Aid for Scientific Research (grant 18K07544 to Y.A.), Grants-in-Aid for Research on Nervous and Mental Disorders (grant 28-6 to Y.A.), and the Japan Agency for Medical Research and Development (grants 17ek0109154h0003, 17am0301021h0003, and 17ek0109239h0001 to Y.A. and S.T.). We thank Dr. Rika Maruyama for scientific advice and Dr. Terence Partridge for providing the H2K-WT and *mdx*52 myoblasts.

REFERENCES

1. Shimizu-Motohashi, Y., Miyatake, S., Komaki, H., Takeda, S., and Aoki, Y. (2016). Recent advances in innovative therapeutic approaches for Duchenne muscular dystrophy: from discovery to clinical trials. Am. J. Transl. Res. *8*, 2471–2489.
2. Aoki, Y., Yokota, T., Nagata, T., Nakamura, A., Tanihata, J., Saito, T., Duguez, S.M., Nagaraju, K., Hoffman, E.P., Partridge, T., and Takeda, S. (2012). Bodywide skipping of exons 45-55 in dystrophic mdx52 mice by systemic antisense delivery. Proc. Natl. Acad. Sci. USA *109*, 13763–13768.
3. Kole, R., Krainer, A.R., and Altman, S. (2012). RNA therapeutics: beyond RNA interference and antisense oligonucleotides. Nat. Rev. Drug Discov. *11*, 125–140.
4. Arora, V., Devi, G.R., and Iversen, P.L. (2004). Neutrally charged phosphorodiamidate morpholino antisense oligomers: uptake, efficacy and pharmacokinetics. Curr. Pharm. Biotechnol. *5*, 431–439.
5. Lu, Q.L., Rabinowitz, A., Chen, Y.C., Yokota, T., Yin, H., Alter, J., Jadoon, A., Bou-Gharios, G., and Partridge, T. (2005). Systemic delivery of antisense oligoribonucleotide restores dystrophin expression in body-wide skeletal muscles. Proc. Natl. Acad. Sci. USA *102*, 198–203.
6. Yokota, T., Lu, Q.L., Partridge, T., Kobayashi, M., Nakamura, A., Takeda, S., and Hoffman, E. (2009). Efficacy of systemic morpholino exon-skipping in Duchenne dystrophy dogs. Ann. Neurol. *65*, 667–676.
7. Guncay, A., and Yokota, T. (2015). Antisense oligonucleotide drugs for Duchenne muscular dystrophy: how far have we come and what does the future hold? Future Med. Chem. *7*, 1631–1635.
8. Touznik, A., Lee, J.J., and Yokota, T. (2014). New developments in exon skipping and splice modulation therapies for neuromuscular diseases. Expert Opin. Biol. Ther. *14*, 809–819.
9. Dowling, J.J. (2016). Eteplirsen therapy for Duchenne muscular dystrophy: skipping to the front of the line. Nat. Rev. Neurol. *12*, 675–676.
10. Zhang, A., Uaesoontrachoon, K., Shaughnessy, C., Das, J.R., Rayavarapu, S., Brown, K.J., Ray, P.E., Nagaraju, K., van den Anker, J.N., Hoffman, E.P., and Hathout, Y. (2015). The use of urinary and kidney SILAM proteomics to monitor kidney response to high dose morpholino oligonucleotides in the mdx mouse. Toxicol. Rep. *2*, 838–849.
11. Amantana, A., Moulton, H.M., Cate, M.L., Reddy, M.T., Whitehead, T., Hassinger, J.N., Youngblood, D.S., and Iversen, P.L. (2007). Pharmacokinetics, biodistribution, stability and toxicity of a cell-penetrating peptide-morpholino oligomer conjugate. Bioconjug. Chem. *18*, 1325–1331.
12. Burki, U., Keane, J., Blain, A., O'Donovan, L., Gait, M.J., Laval, S.H., and Straub, V. (2015). Development and application of an ultrasensitive hybridization-based ELISA method for the determination of peptide-conjugated phosphorodiamidate morpholino oligonucleotides. Nucleic Acid Ther. *25*, 275–284.
13. Fröhlich, E. (2012). The role of surface charge in cellular uptake and cytotoxicity of medical nanoparticles. Int. J. Nanomedicine *7*, 5577–5591.
14. Petrof, B.J., Shrager, J.B., Stedman, H.H., Kelly, A.M., and Sweeney, H.L. (1993). Dystrophin protects the sarcolemma from stresses developed during muscle contraction. Proc. Natl. Acad. Sci. USA *90*, 3710–3714.
15. McArdle, A., Edwards, R.H., and Jackson, M.J. (1994). Time course of changes in plasma membrane permeability in the dystrophin-deficient mdx mouse. Muscle Nerve *17*, 1378–1384.
16. Aoki, Y., Nagata, T., Yokota, T., Nakamura, A., Wood, M.J., Partridge, T., and Takeda, S. (2013). Highly efficient in vivo delivery of PMO into regenerating myotubes and rescue in laminin-α2 chain-null congenital muscular dystrophy mice. Hum. Mol. Genet. *22*, 4914–4928.
17. Novak, J.S., Hogarth, M.W., Boehler, J.F., Nearing, M., Vila, M.C., Heredia, R., Fiorillo, A.A., Zhang, A., Hathout, Y., Hoffman, E.P., et al. (2017). Myoblasts and macrophages are required for therapeutic morpholino antisense oligonucleotide delivery to dystrophic muscle. Nat. Commun. *8*, 941.
18. Han, G., Gu, B., Cao, L., Gao, X., Wang, Q., Seow, Y., Zhang, N., Wood, M.J., and Yin, H. (2016). Hexose enhances oligonucleotide delivery and exon skipping in dystrophin-deficient mdx mice. Nat. Commun. *7*, 10981.
19. Ezzat, K., Aoki, Y., Koo, T., McClorey, G., Benner, L., Coenen-Stass, A., O'Donovan, L., Lehto, T., Garcia-Guerra, A., Nordin, J., et al. (2015). Self-assembly into nanoparticles is essential for receptor mediated uptake of therapeutic antisense oligonucleotides. Nano Lett. *15*, 4364–4373.
20. Canton, J., Neculai, D., and Grinstein, S. (2013). Scavenger receptors in homeostasis and immunity. Nat. Rev. Immunol. *13*, 621–634.
21. Platt, N., and Gordon, S. (1998). Scavenger receptors: diverse activities and promiscuous binding of polyanionic ligands. Chem. Biol. *5*, R193–R203.
22. Tinsley, J., Deconinck, N., Fisher, R., Kahn, D., Phelps, S., Gillis, J.M., and Davies, K. (1998). Expression of full-length utrophin prevents muscular dystrophy in mdx mice. Nat. Med. *4*, 1441–1444.
23. Plüddemann, A., Neyen, C., and Gordon, S. (2007). Macrophage scavenger receptors and host-derived ligands. Methods *43*, 207–217.
24. Arnida, Janát-Amsbury, M.M., Ray, A., Peterson, C.M., and Ghandehari, H. (2011). Geometry and surface characteristics of gold nanoparticles influence their biodistribution and uptake by macrophages. Eur. J. Pharm. Biopharm. *77*, 417–423.
25. Jordy, A.B., and Kiens, B. (2014). Regulation of exercise-induced lipid metabolism in skeletal muscle. Exp. Physiol. *99*, 1586–1592.
26. DeWitte-Orr, S.J., Collins, S.E., Bauer, C.M., Bowdish, D.M., and Mossman, K.L. (2010). An accessory to the 'Trinity': SR-As are essential pathogen sensors of extracellular dsRNA, mediating entry and leading to subsequent type I IFN responses. PLoS Pathog. *6*, e1000829.
27. Bowdish, D.M., and Gordon, S. (2009). Conserved domains of the class A scavenger receptors: evolution and function. Immunol. Rev. *227*, 19–31.
28. Lehto, T., Castillo Alvarez, A., Gauck, S., Gait, M.J., Coursindel, T., Wood, M.J., Lebleu, B., and Boisguerin, P. (2014). Cellular trafficking determines the exon skipping activity of Pip6a-PMO in mdx skeletal and cardiac muscle cells. Nucleic Acids Res. *42*, 3207–3217.
29. Betts, C., Saleh, A.F., Arzumanov, A.A., Hammond, S.M., Godfrey, C., Coursindel, T., Gait, M.J., and Wood, M.J. (2012). Pip6-PMO, a new generation of peptide-oligonucleotide conjugates with improved cardiac exon skipping activity for DMD treatment. Mol. Ther. Nucleic Acids *1*, e38.
30. Miyatake, S., Mizobe, Y., Takizawa, H., Hara, Y., Yokota, T., Takeda, S., and Aoki, Y. (2018). Exon skipping therapy using phosphorodiamidate morpholino oligomers in the mdx52 mouse model of Duchenne muscular dystrophy. Methods Mol. Biol. *1687*, 123–141.
31. Heemskerk, H., de Winter, C., van Kuik, P., Heuvelmans, N., Sabatelli, P., Rimessi, P., Braghetta, P., van Ommen, G.J., de Kimpe, S., Ferlini, A., et al. (2010). Preclinical PK and PD studies on 2′-O-methyl-phosphorothioate RNA antisense oligonucleotides in the mdx mouse model. Mol. Ther. *18*, 1210–1217.
32. Hoffman, E.P., Bronson, A., Levin, A.A., Takeda, S., Yokota, T., Baudy, A.R., and Connor, E.M. (2011). Restoring dystrophin expression in duchenne muscular dystrophy muscle progress in exon skipping and stop codon read through. Am. J. Pathol. *179*, 12–22.
33. Peiser, L., and Gordon, S. (2001). The function of scavenger receptors expressed by macrophages and their role in the regulation of inflammation. Microbes Infect. *3*, 149–159.
34. Mokri, B., and Engel, A.G. (1975). Duchenne dystrophy: electron microscopic findings pointing to a basic or early abnormality in the plasma membrane of the muscle fiber. Neurology *25*, 1111–1120.
35. Shibuya, S., Wakayama, Y., Inoue, M., Oniki, H., and Kominami, E. (2002). Changes in the distribution and density of caveolin 3 molecules at the plasma membrane of mdx mouse skeletal muscles: a fracture-label electron microscopic study. Neurosci. Lett. *325*, 171–174.
36. Galbiati, F., Volonte, D., Engelman, J.A., Scherer, P.E., and Lisanti, M.P. (1999). Targeted down-regulation of caveolin-3 is sufficient to inhibit myotube formation in differentiating C2C12 myoblasts. Transient activation of p38 mitogen-activated protein kinase is required for induction of caveolin-3 expression and subsequent myotube formation. J. Biol. Chem. *274*, 30315–30321.
37. Stoppani, E., Rossi, S., Meacci, E., Penna, F., Costelli, P., Bellucci, A., Faggi, F., Maiolo, D., Monti, E., and Fanzani, A. (2011). Point mutated caveolin-3 form (P104L) impairs myoblast differentiation via Akt and p38 signalling reduction, leading to an immature cell signature. Biochim. Biophys. Acta *1812*, 468–479.

38. Aoki, Y., Nakamura, A., Yokota, T., Saito, T., Okazawa, H., Nagata, T., and Takeda, S. (2010). In-frame dystrophin following exon 51-skipping improves muscle pathology and function in the exon 52-deficient mdx mouse. Mol. Ther. *18*, 1995–2005.

39. Vadali, S., and Post, S.R. (2014). Lipid rafts couple class A scavenger receptors to phospholipase A2 activation during macrophage adhesion. J. Leukoc. Biol. *96*, 873–881.

40. Post, S.R., Gass, C., Rice, S., Nikolic, D., Crump, H., and Post, G.R. (2002). Class A scavenger receptors mediate cell adhesion via activation of G(i/o) and formation of focal adhesion complexes. J. Lipid Res. *43*, 1829–1836.

41. Tierney, M.T., and Sacco, A. (2016). Inducing and evaluating skeletal muscle injury by notexin and barium chloride. Methods Mol. Biol. *1460*, 53–60.

42. Arechavala-Gomeza, V., Graham, I.R., Popplewell, L.J., Adams, A.M., Aartsma-Rus, A., Kinali, M., Morgan, J.E., van Deutekom, J.C., Wilton, S.D., Dickson, G., and Muntoni, F. (2007). Comparative analysis of antisense oligonucleotide sequences for targeted skipping of exon 51 during dystrophin pre-mRNA splicing in human muscle. Hum. Gene Ther. *18*, 798–810.

43. Florence, J.M., Fox, P.T., Planer, G.J., and Brooke, M.H. (1985). Activity, creatine kinase, and myoglobin in Duchenne muscular dystrophy: a clue to etiology? Neurology *35*, 758–761.

44. Repetto, S., Bado, M., Broda, P., Lucania, G., Masetti, E., Sotgia, F., Carbone, I., Pavan, A., Bonilla, E., Cordone, G., et al. (1999). Increased number of caveolae and caveolin-3 overexpression in Duchenne muscular dystrophy. Biochem. Biophys. Res. Commun. *261*, 547–550.

45. Shibuya, S., Wakayama, Y., Murahashi, M., Kojima, H., Oniki, H., Matsuzaki, T., and Nonaka, I. (2001). Muscle plasma membrane changes in dystrophin gene exon 52 knockout mouse. Pathol. Res. Pract. *197*, 441–447.

46. Vistisen, B., Roepstorff, K., Roepstorff, C., Bonen, A., van Deurs, B., and Kiens, B. (2004). Sarcolemmal FAT/CD36 in human skeletal muscle colocalizes with caveolin-3 and is more abundant in type 1 than in type 2 fibers. J. Lipid Res. *45*, 603–609.

47. Poussard, S., Decossas, M., Le Bihan, O., Mornet, S., Naudin, G., and Lambert, O. (2015). Internalization and fate of silica nanoparticles in C2C12 skeletal muscle cells: evidence of a beneficial effect on myoblast fusion. Int. J. Nanomedicine *10*, 1479–1492.

48. Miyatake, S., Shimizu-Motohashi, Y., Takeda, S., and Aoki, Y. (2016). Anti-inflammatory drugs for Duchenne muscular dystrophy: focus on skeletal muscle-releasing factors. Drug Des. Devel. Ther. *10*, 2745–2758.

49. Butler, M., Crooke, R.M., Graham, M.J., Lemonidis, K.M., Lougheed, M., Murray, S.F., Witchell, D., Steinbrecher, U., and Bennett, C.F. (2000). Phosphorothioate oligodeoxynucleotides distribute similarly in class A scavenger receptor knockout and wild-type mice. J. Pharmacol. Exp. Ther. *292*, 489–496.

50. Miller, C.M., Donner, A.J., Blank, E.E., Egger, A.W., Kellar, B.M., Østergaard, M.E., Seth, P.P., and Harris, E.N. (2016). Stabilin-1 and Stabilin-2 are specific receptors for the cellular internalization of phosphorothioate-modified antisense oligonucleotides (ASOs) in the liver. Nucleic Acids Res. *44*, 2782–2794.

51. Dirin, M., and Winkler, J. (2013). Influence of diverse chemical modifications on the ADME characteristics and toxicology of antisense oligonucleotides. Expert Opin. Biol. Ther. *13*, 875–888.

52. Kerr, M.C., and Teasdale, R.D. (2009). Defining macropinocytosis. Traffic *10*, 364–371.

53. Nagayama, S., Ogawara, K., Minato, K., Fukuoka, Y., Takakura, Y., Hashida, M., Higaki, K., and Kimura, T. (2007). Fetuin mediates hepatic uptake of negatively charged nanoparticles via scavenger receptor. Int. J. Pharm. *329*, 192–198.

54. Ezzat, K., Helmfors, H., Tudoran, O., Juks, C., Lindberg, S., Padari, K., El-Andaloussi, S., Pooga, M., and Langel, U. (2012). Scavenger receptor-mediated uptake of cell-penetrating peptide nanocomplexes with oligonucleotides. FASEB J. *26*, 1172–1180.

55. Saleh, A.F., Arzumanov, A.A., and Gait, M.J. (2012). Overview of alternative oligonucleotide chemistries for exon skipping. Methods Mol. Biol. *867*, 365–378.

56. Echigoya, Y., Mouly, V., Garcia, L., Yokota, T., and Duddy, W. (2015). In silico screening based on predictive algorithms as a design tool for exon skipping oligonucleotides in Duchenne muscular dystrophy. PLoS ONE *10*, e0120058.

57. Araki, E., Nakamura, K., Nakao, K., Kameya, S., Kobayashi, O., Nonaka, I., Kobayashi, T., and Katsuki, M. (1997). Targeted disruption of exon 52 in the mouse dystrophin gene induced muscle degeneration similar to that observed in Duchenne muscular dystrophy. Biochem. Biophys. Res. Commun. *238*, 492–497.

58. Suzuki, H., Kurihara, Y., Takeya, M., Kamada, N., Kataoka, M., Jishage, K., Ueda, O., Sakaguchi, H., Higashi, T., Suzuki, T., et al. (1997). A role for macrophage scavenger receptors in atherosclerosis and susceptibility to infection. Nature *386*, 292–296.

59. Ono, Y., Boldrin, L., Knopp, P., Morgan, J.E., and Zammit, P.S. (2010). Muscle satellite cells are a functionally heterogeneous population in both somite-derived and branchiomeric muscles. Dev. Biol. *337*, 29–41.

60. Echigoya, Y., Nakamura, A., Nagata, T., Urasawa, N., Lim, K.R.Q., Trieu, N., Panesar, D., Kuraoka, M., Moulton, H.M., Saito, T., et al. (2017). Effects of systemic multiexon skipping with peptide-conjugated morpholinos in the heart of a dog model of Duchenne muscular dystrophy. Proc. Natl. Acad. Sci. USA *114*, 4213–4218.